

## NMR, IR/Raman, and Structural Properties in HNO and RNO (R = Alkyl and Aryl) Metalloporphyrins with Implication for the HNO–Myoglobin Complex

Yan Ling, Christopher Mills, Rebecca Weber, Liu Yang, and Yong Zhang\*

Department of Chemistry and Biochemistry, University of Southern Mississippi, 118 College Drive #5043, Hattiesburg, Mississippi 39406

Received August 31, 2009; E-mail: yong.zhang@usm.edu

**Abstract:** Structural and functional details of heme protein complexes with HNO and the isoelectronic RNO (R = alkyl and aryl) molecules (metabolic intermediates) are largely unknown. We report a quantum chemical investigation of three characteristic spectroscopic properties,  $^1\text{H}$  and  $^{15}\text{N}$  NMR chemical shifts and NO vibrational frequencies in synthetic HNO and RNO heme complexes, with theory-versus-experiment correlation coefficients  $R^2 = 0.990\text{--}0.998$ . A new density functional theory (DFT) method was found to yield excellent predictions of experimental structures of HNO, RNO, and NO heme systems. Interestingly, this method also helps the identification of an excellent linear quantitative structure observable relationship between NO vibrational frequencies and bond lengths in all of these NO-containing systems. This suggests that NO vibrations are largely local effects of the NO bonds in these complexes and may help deduce the NO bond lengths from using experimental vibrational data in these systems. The NO vibrational frequencies in HNO, RNO, and NO metalloporphyrins were found to follow a general trend of  $\text{NO} > \text{RNO} > \text{HNO}$  complexes, as a result of the electron populations in the antibonding NO orbitals of  $\text{NO} < \text{RNO} < \text{HNO}$  complexes. Investigations of the NMR and IR/Raman spectroscopic data in HNO metal complexes show that HNO is a strong  $\pi$ -acid. In addition, we performed the first quantum chemical investigation of the hydrogen-bond effect on HNO in MbHNO (Mb = myoglobin) models. On the basis of comparisons with experimental  $^1\text{H}$  and  $^{15}\text{N}$  NMR results and NO vibrational frequency in MbHNO, a dual hydrogen-bond mode for HNO in MbHNO was proposed. The enhanced stability from this dual hydrogen bonding may provide a basis for the unusual stability of MbHNO observed experimentally. These results should facilitate spectroscopic characterizations and structural investigations of HNO and RNO heme proteins and models.

### Introduction

HNO, nitroxyl or nitrosyl hydride, is a sibling molecule of the well-known signaling agent nitric oxide (NO), yet their chemistries are quite different.<sup>1</sup> For instance, HNO and NO can lead to increases in the biochemical messengers cyclic adenosine monophosphate (cAMP) and cyclic guanosine monophosphate (cGMP), respectively.<sup>2</sup> HNO participates in many physiological and pathological processes.<sup>2–8</sup> With a more favorable vasodilative effect than NO and an increased contractility effect, HNO donors offer a promising new class of vasodilators and heart

failure treatment.<sup>9</sup> HNO has also been suggested as a potential pharmacological treatment for reduction of neuronal damage, for instance, during stroke.<sup>2</sup> These observations strongly suggest that HNO has distinctive roles in biology and medicine. Heme proteins have long been proposed to mediate the physiological activity of HNO, since the early studies of biological denitrification processes in plants, bacteria, and fungi catalyzed by nitrite and nitric oxide reductases.<sup>10,11</sup> HNO has also been proposed in the catalytic cycles of the heme enzyme nitric oxide synthase, peroxidase, and cytochrome P450.<sup>12–15</sup> The isoelectronic RNO molecules (R = alkyl or aryl groups) that are metabolic intermediates of the amines, hydroxylamines, and organic nitro compounds have been found to bind with a number of heme proteins, such as myoglobin, soluble guanylyl cyclase,

- (1) Wilson, E. K. *Chem. Eng. News* **2004**, *82*, 39–44.
- (2) Miranda, K. M. *Coord. Chem. Rev.* **2005**, *249*, 433–455.
- (3) Ma, X. L.; Cao, F.; Liu, G. L.; Lopez, B. L.; Christopher, T. A.; Fukuto, J. M.; Wink, D. A.; Feelisch, M. *Proc. Natl. Acad. Sci. U.S.A.* **1999**, *96*, 14617–14622.
- (4) Boje, K. M. K.; Lakhman, S. S. *J. Pharmacol. Exp. Ther.* **2000**, *293*, 545–550.
- (5) Booth, B. P.; Tabrizi-Fard, M. A.; Fung, H. L. *Biochem. Pharmacol.* **2000**, *59*, 1603–1609.
- (6) Nagasawa, H. T.; Demaster, E. G.; Redfern, B.; Shirota, F. N.; Goon, J. W. *J. Med. Chem.* **1990**, *33*, 3120–3122.
- (7) Sidorkina, O.; Espey, M. G.; Miranda, K. M.; Wink, D. A.; Laval, J. *Free Radical Biol. Med.* **2003**, *35*, 1431–1438.
- (8) Shinyashiki, M.; Chiang, K. T.; Switzer, C. H.; Gralla, E. B.; Valentine, J. S.; Thiele, D. J.; Fukuto, J. M. *Proc. Natl. Acad. Sci. U.S.A.* **2000**, *97*, 2491–2496.

- (9) Feelisch, M. *Proc. Natl. Acad. Sci. U.S.A.* **2003**, *100*, 4978–4980.
- (10) Averill, B. A. *Chem. Rev.* **1996**, *96*, 2951–2964.
- (11) Farmer, P. J.; Sulc, F. *J. Inorg. Biochem.* **2005**, *99*, 166–184.
- (12) Rusche, K. M.; Spiering, M. M.; Marletta, M. A. *Biochemistry* **1998**, *37*, 15503–15512.
- (13) Miranda, K. M.; Paolucci, N.; Katori, T.; Thomas, D. D.; Wink, D. A. *J. Inorg. Biochem.* **2003**, *96*, 49–49.
- (14) Huang, J. M.; Sommers, E. M.; Kim-Shapiro, D. B.; King, S. B. *J. Am. Chem. Soc.* **2002**, *124*, 3473–3480.
- (15) Miranda, K. M.; Paolucci, N.; Katori, T.; Thomas, D. D.; Ford, E.; Bartberger, M. D.; Espey, M. G.; Kass, D. A.; Feelisch, M.; Fukuto, J. M.; Wink, D. A. *Proc. Natl. Acad. Sci. U.S.A.* **2003**, *100*, 9196–9201.

catalase, and cytochrome P450.<sup>16–18</sup> However, many structural and functional details of HNO or RNO protein complexes are still unknown.

Spectroscopic investigations of HNO and RNO protein complexes and synthetic models can provide useful information to help characterize these systems. Recently, an unusually stable HNO adduct of myoglobin (MbHNO) was isolated,<sup>19,20</sup> which enabled NMR, resonance Raman, and X-ray absorption spectroscopic characterizations.<sup>21,22</sup> The <sup>1</sup>H NMR chemical shift of 14.8 ppm is a unique feature for the HNO moiety in MbHNO. A more recent investigation of HNO complexes with other oxygen-binding hemoglobins supports that this proton NMR shift can serve as a sensitive probe of the heme active site.<sup>23</sup> Interestingly, this shift also varies with the metal center and ligand set in synthetic HNO metal complexes,<sup>24–33</sup> suggesting a useful role in characterizing synthetic HNO metal systems, too. The <sup>15</sup>N NMR chemical shifts of the HNO moieties in a number of HNO heme protein complexes were also found to vary with the specific protein environment,<sup>23</sup> and they are different from the nitrogen shifts observed in RNO iron porphyrin complexes.<sup>34</sup> In addition, experimental studies suggest that the NO vibrational frequency,  $\nu_{\text{NO}}$ , is another useful probe of the metal environment in both HNO and RNO heme complexes. For example,  $\nu_{\text{NO}}$  in MbHNO is 1385 cm<sup>-1</sup>, which is quite different from that of the nitrosyl ferrous Mb, 1613 cm<sup>-1</sup>, and that of the nitrosyl ferric Mb, 1927 cm<sup>-1</sup>.<sup>22</sup> The experimental NO vibrational frequencies in HNO metal complexes have a broad range of 1335–1493 cm<sup>-1</sup>, with that in a heme model system (1380 cm<sup>-1</sup>) being close to the value seen in MbHNO.<sup>24–33</sup> In contrast, the NO vibrational frequencies in RNO iron porphyrin complexes<sup>35,36</sup> (1400–1445 cm<sup>-1</sup>) are

relatively higher than those in HNO heme complexes. Therefore, the <sup>1</sup>H and <sup>15</sup>N NMR chemical shifts and NO vibrational frequencies are important spectroscopic probes to investigate HNO and RNO heme systems.

However, there are no quantum chemical investigations of the characteristic <sup>1</sup>H NMR shifts in HNO protein or model systems. For the <sup>15</sup>N NMR shifts in HNO or RNO protein and model systems, there is a previous computational investigation of some RNO metalloporphyrins, which provides a useful analysis of the solid-state <sup>15</sup>N NMR results, yet the predicted isotropic shifts in many iron porphyrins have 30 ppm or larger errors.<sup>34</sup> Regarding  $\nu_{\text{NO}}$  calculations, a recent investigation of MbHNO using the simple [Fe(Por)(ImH)(HNO)] (Por = porphyrinate) model suggests that quantum chemical investigations may be helpful to understand the experimental vibrational spectra,<sup>37</sup> as with other NO heme complexes.<sup>38–41</sup> However, errors of 31–32 cm<sup>-1</sup> for the NO vibrational frequency in MbHNO from the best reported calculations clearly indicate the insufficiency of the used model or method. Another report of the gas-phase  $\nu_{\text{NO}}$  calculation is for a synthetic HNO metal complex Ru(HNO)(‘py<sup>bu</sup>S<sub>4</sub>’) (‘py<sup>bu</sup>S<sub>4</sub>’ = 2,6-bis(2-mercapto-3,5-di-*tert*-butylphenylthio)dimethyl-pyridine),<sup>30</sup> with an error of 155 cm<sup>-1</sup> and a surprisingly large effect of ~120 cm<sup>-1</sup> on the calculated  $\nu_{\text{NO}}$  from using hydrogen bonds. In addition, there are no reports of quantum chemical investigations of NO vibrational frequencies in RNO heme models. Overall, high accuracy predictions of the <sup>1</sup>H and <sup>15</sup>N NMR chemical shifts and NO vibrational frequencies as important spectroscopic probes to investigate HNO and RNO heme systems have not been reported yet.

Previous investigations show that the high accuracy predictions of some characteristic spectroscopic observables can help understand, assign, and sometimes correct experimental spectra,<sup>42,43</sup> help understand relevant electronic structures,<sup>42,44–52</sup> and provide a valuable venue to refine or determine protein structures<sup>46,48,49,51,53,54</sup> using a way we now call the integrated quantum mechanics and spectroscopy (QM/S) approach. This is based on an intrinsic mathematical relationship between a

- (16) Lee, J.; Chen, L.; West, A. H.; Richter-Addo, G. B. *Chem. Rev.* **2002**, *102*, 1019–1065.
- (17) Copeland, D. M.; West, A. H.; Richter-Addo, G. B. *Proteins: Struct., Funct., Genet.* **2003**, *53*, 182–192.
- (18) Arutyunyan, E. G.; Kuranova, I. P.; Vainshtein, B. K.; Steigemann, W. *Kristallografiya* **1982**, *25*, 80.
- (19) Lin, R.; Farmer, P. J. *J. Am. Chem. Soc.* **2000**, *122*, 2393–2394.
- (20) Sulc, F.; Immoos, C. E.; Pervitsky, D.; Farmer, P. J. *J. Am. Chem. Soc.* **2004**, *126*, 1096–1101.
- (21) Sulc, F.; Fleischer, E.; Farmer, P. J.; Ma, D. J.; La Mar, G. N. *J. Biol. Inorg. Chem.* **2003**, *8*, 348–352.
- (22) Immoos, C. E.; Sulc, F.; Farmer, P. J.; Czarniecki, K.; Bocian, D. F.; Levina, A.; Aitken, J. B.; Armstrong, R. S.; Lay, P. A. *J. Am. Chem. Soc.* **2005**, *127*, 814–815.
- (23) Kumar, M. R.; Pervitsky, D.; Chen, L.; Poulos, T.; Kundu, S.; Hargrove, M. S.; Rivera, E. J.; Diaz, A.; Colon, J. L.; Farmer, P. J. *Biochemistry* **2009**, *48*, 5018–5025.
- (24) Grundy, K. R.; Reed, C. A.; Roper, W. R. *J. Chem. Soc. D: Chem. Commun.* **1970**, 1501–1502.
- (25) Wilson, R. D.; Ibers, J. A. *Inorg. Chem.* **1979**, *18*, 336–343.
- (26) Melenkivitz, R.; Hillhouse, G. L. *Chem. Commun.* **2002**, 660–661.
- (27) Southern, J. S.; Green, M. T.; Hillhouse, G. L.; Guzei, I. A.; Rheingold, A. L. *Inorg. Chem.* **2001**, *40*, 6039–6046.
- (28) Southern, J. S.; Hillhouse, G. L.; Rheingold, A. L. *J. Am. Chem. Soc.* **1997**, *119*, 12406–12407.
- (29) Melenkivitz, R.; Southern, J. S.; Hillhouse, G. L.; Concolino, T. E.; Liable-Sands, L. M.; Rheingold, A. L. *J. Am. Chem. Soc.* **2002**, *124*, 12068–12069.
- (30) Sellmann, D.; Gottschalk-Gaudig, T.; Haussinger, D.; Heinemann, F. W.; Hess, B. A. *Chem.-Eur. J.* **2001**, *7*, 2099–2103.
- (31) Marchenko, A. V.; Vedernikov, A. N.; Dye, D. F.; Pink, M.; Zaleski, J. M.; Caulton, K. G. *Inorg. Chem.* **2002**, *41*, 4087–4089.
- (32) Marchenko, A. V.; Vedernikov, A. N.; Dye, D. F.; Pink, M.; Zaleski, J. M.; Caulton, K. G. *Inorg. Chem.* **2004**, *43*, 351–360.
- (33) Lee, J. Y.; Richter-Addo, G. B. *J. Inorg. Biochem.* **2004**, *98*, 1247–1250.
- (34) Godbout, N.; Sanders, L. K.; Salzmann, R.; Havlin, R. H.; Wojdelski, M.; Oldfield, E. *J. Am. Chem. Soc.* **1999**, *121*, 3829–3844.
- (35) Sohl, C. D.; Lee, J. Y.; Alguindigue, S. S.; Khan, M. A.; Richter-Addo, G. B. *J. Inorg. Biochem.* **2004**, *98*, 1238–1246.

- (36) Mansuy, D.; Battioni, P.; Chottard, J. C.; Riche, C.; Chiaroni, A. *J. Am. Chem. Soc.* **1983**, *105*, 455–463.
- (37) Linder, D. P.; Rodgers, K. R. *Inorg. Chem.* **2005**, *44*, 8259–8264.
- (38) Praneeth, V. K. K.; Haupt, E.; Lehnert, N. *J. Inorg. Biochem.* **2005**, *99*, 940–948.
- (39) Linder, D. P.; Rodgers, K. R. *Inorg. Chem.* **2005**, *44*, 1367–1380.
- (40) Xu, C. L.; Spiro, T. G. *J. Biol. Inorg. Chem.* **2008**, *13*, 613–621.
- (41) Linder, D. P.; Rodgers, K. R.; Banister, J.; Wyllie, G. R. A.; Ellison, M. K.; Scheidt, W. R. *J. Am. Chem. Soc.* **2004**, *126*, 14136–14148.
- (42) Mao, J. H.; Zhang, Y.; Oldfield, E. *J. Am. Chem. Soc.* **2002**, *124*, 13911–13920.
- (43) Zhang, Y.; Mukherjee, S.; Oldfield, E. *J. Am. Chem. Soc.* **2005**, *127*, 2370–2371.
- (44) Zhang, Y.; Mao, J. H.; Oldfield, E. *J. Am. Chem. Soc.* **2002**, *124*, 7829–7839.
- (45) Zhang, Y.; Mao, J. H.; Godbout, N.; Oldfield, E. *J. Am. Chem. Soc.* **2002**, *124*, 13921–13930.
- (46) Zhang, Y.; Gossman, W.; Oldfield, E. *J. Am. Chem. Soc.* **2003**, *125*, 16387–16396.
- (47) Zhang, Y.; Oldfield, E. *J. Phys. Chem. A* **2003**, *107*, 4147–4150.
- (48) Zhang, Y.; Oldfield, E. *J. Am. Chem. Soc.* **2004**, *126*, 9494–9495.
- (49) Zhang, Y.; Oldfield, E. *J. Am. Chem. Soc.* **2004**, *126*, 4470–4471.
- (50) Kervern, G.; Pintacuda, G.; Zhang, Y.; Oldfield, E.; Roukoss, C.; Kuntz, E.; Herdtweck, E.; Basset, J. M.; Cadars, S.; Lesage, A.; Coperet, C.; Emsley, L. *J. Am. Chem. Soc.* **2006**, *128*, 13545–13552.
- (51) Zhang, Y.; Oldfield, E. *J. Am. Chem. Soc.* **2008**, *130*, 3814–3823.
- (52) Ling, Y.; Zhang, Y. *J. Am. Chem. Soc.* **2009**, *131*, 6386–6388.
- (53) Mao, J. H.; Mukherjee, S.; Zhang, Y.; Cao, R.; Sanders, J. M.; Song, Y. C.; Zhang, Y. H.; Meints, G. A.; Gao, Y. G.; Mukkamala, D.; Hudock, M. P.; Oldfield, E. *J. Am. Chem. Soc.* **2006**, *128*, 14485–14497.

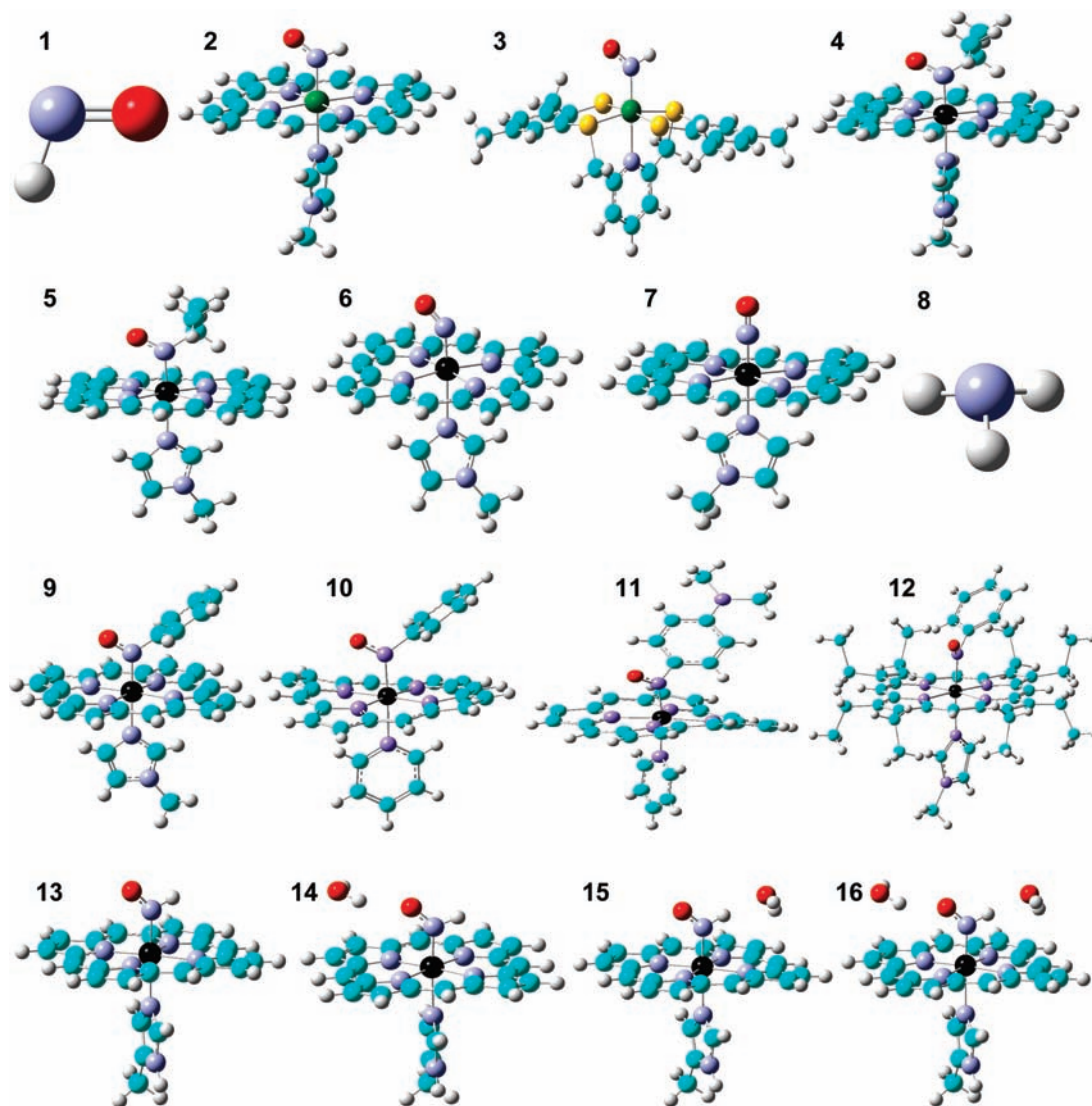


**Figure 1.** Structures of the molecules (1–16) investigated in this work. Atom color scheme: Ru, dark green; Fe, black; C, cyan; N, blue; O, red; S, yellow; H, gray.

spectroscopic observable of a given molecule and its molecular structure. According to a fundamental theorem in the density functional theory (DFT), the Hohenberg–Kohn theorem,<sup>55</sup> any property can be expressed by a functional of the molecular system's electron density. Therefore, a spectroscopic observable property (e.g., NMR chemical shift) is a functional of the electron density,  $\rho(\mathbf{r}_1, \mathbf{r}_2, \dots, \mathbf{r}_n)$ , which is determined by the molecular structure or spatial arrangement of the atoms ( $n$  atoms) in this molecule,  $(\mathbf{r}_1, \mathbf{r}_2, \dots, \mathbf{r}_n)$ . In many cases, this quantitative structure observable relationship (QSOR) cannot be expressed explicitly, so quantum chemical geometry optimization is needed to find the optimal structure that can minimize the prediction errors for some key experimental spectroscopic observables.<sup>48,49,53</sup> In addition to the use of this implicit QSOR approach, sometimes, numerical explicit QSOR may be constructed, and a probability surface can be used to directly find the optimal geometric parameters.<sup>46,54</sup> The easiest way to determine a geometric parameter from using the experimental spectroscopic

data may be the use of an analytic QSOR, which is actually not uncommon, for example, the well-known Karplus relationship.<sup>56</sup>

Here, we report a quantum chemical investigation of the <sup>1</sup>H and <sup>15</sup>N NMR chemical shifts and NO vibrational frequencies in synthetic HNO and RNO heme complexes, with prediction errors  $\sim 2\text{--}3\%$  of the experimental data ranges, using a new DFT method based on a comprehensive investigation. An analytic QSOR was found between the NO vibrational frequencies and the NO bond lengths in all HNO, RNO, and NO heme systems investigated here. In addition, on the basis of comparisons with these three experimental spectroscopic data of MbHNO, a dual hydrogen-bond mode for HNO in MbHNO was proposed for the first time, using model systems. These results should facilitate future studies of HNO and RNO metalloporphyrins and heme proteins.

### Computational Details

As shown in Figure 1, 16 molecules were investigated to evaluate the predictions of the characteristic spectroscopic probes in HNO and

(54) McMahon, M. T.; deDios, A. C.; Godbout, N.; Salzmann, R.; Laws, D. D.; Le, H. B.; Havlin, R. H.; Oldfield, E. *J. Am. Chem. Soc.* **1998**, *120*, 4784–4797.

(55) Hohenberg, P.; Kohn, W. *Phys. Rev. B* **1964**, *136*, 864–871.

(56) Karplus, M. *J. Am. Chem. Soc.* **1963**, *85*, 2870–2871.

RNO heme models and other relevant systems: HNO (**1**), Ru-(TTP)(HNO)(1-MeIm) (**2**), Ru(HNO)(“py<sup>bu</sup>S<sub>4</sub>”) (**3**), Fe(TPP)(<sup>i</sup>PrNO)(1-MeIm) (**4**), Fe(OEP)(<sup>i</sup>PrNO)(1-MeIm) (**5**), Fe(TPP)(NO)(1-MeIm) (**6**), [Fe(OETPP)(NO)(1-MeIm)]<sup>+</sup> (**7**), NH<sub>3</sub> (**8**), Fe(TPP)(PhNO)(1-MeIm) (**9**), Fe(TPP)(PhNO)(py) (**10**), Fe(TPP)(NODMA)(py) (**11**), Fe(OEP)(PhNO)(1-MeIm) (**12**), Fe(Por)(HNO)(5-MeIm) (**13**), Fe(Por)(HNO⋯H<sub>2</sub>O)(5-MeIm) (**14**), Fe(Por)(H<sub>2</sub>O⋯HNO)(5-MeIm) (**15**), and Fe(Por)(H<sub>2</sub>O⋯HNO⋯H<sub>2</sub>O)(5-MeIm) (**16**), where TTP = 5,10,15,20-tetratoylporphyrinato, TPP = 5,10,15,20-tetraphenylporphyrinato, OEP = 2,3,7,8,12,13,17,18-octaethylporphyrinato, OETPP = 2,3,7,8,12,13,17,18-octaethyl-5,10,15,20-tetraphenylporphyrinato, 1-MeIm = 1-methylimidazole, 5-MeIm = 5-methylimidazole, py = pyridine, and NODMA = 4-nitroso-*N,N*-dimethylaniline. The peripheral substituents on the porphyrin rings were replaced by hydrogen atoms as in the previous work<sup>42,44–46,49,54,57</sup> unless otherwise indicated. Molecules **1–8** and **13–16** were subject to full geometry optimizations and subsequent frequency calculations to verify that they are the minimum energy states in their potential energy surfaces. No scaling factors were used in the reported vibrational frequencies. The solution NMR chemical shifts calculations and atomic charges from the natural population analysis<sup>58</sup> (NPA) were done using the fully optimized structures. Solid-state NMR chemical shifts results of complexes **9–12** were predicted using the corresponding X-ray crystal structures.<sup>34</sup> The calculated <sup>1</sup>H and <sup>15</sup>N NMR chemical shifts are referenced to the calculated chemical shieldings in experimentally used reference standards TMS and NH<sub>3</sub>, respectively.

A comprehensive investigation on the computational methods was performed to evaluate the predictions of structures and various spectroscopic properties of molecules **1–12**, and the selected methods were then used to investigate MbHNO models **13–16**. In addition to the use of two commonly used hybrid Hartree–Fock/density functional theory (HF-DFT) methods B3LYP<sup>59</sup> and mPW1PW91,<sup>60</sup> we examined three series of customized combinations of pure DFT methods. The first series uses the Becke<sup>61</sup> (abbreviated as B) exchange functional with the following correlation functionals: VWN,<sup>62</sup> VWN5,<sup>62</sup> LYP,<sup>63</sup> PL,<sup>64</sup> P86,<sup>65</sup> B95,<sup>66</sup> PBE,<sup>67</sup> TPSS,<sup>68</sup> as implemented in Gaussian 03.<sup>69</sup> The second series uses the Perdew–Wang 1991 exchange functional as modified by the Adamo and Barone (mPW)<sup>60</sup> exchange functional, with the above correlation functionals. The third series of pure DFT methods was built by using the following exchange functionals with the P86<sup>65</sup> correlation functional: G96,<sup>70</sup> PW91,<sup>71</sup> PBE,<sup>67</sup> and O<sup>72</sup> as implemented in Gaussian 03. For nonmetal elements, 30 Pople-type basis sets (from 6-311G(d) to 6-311++G(3df,3pd)) as well as four Dunning’s correlation consistent basis sets<sup>73</sup> (cc-pvdz, aug-ccpvdz, aug-ccpvtz, aug-ccpvqz) were used. For metal elements,

both the all-electron basis sets (Wachters<sup>74,75</sup> and DGDZVP<sup>76</sup>) and the effective core potential basis sets (LanL2DZ,<sup>77</sup> CEP-121G,<sup>78</sup> SDD<sup>79</sup>) were studied.

The use of pure or hybrid DFT methods with different exchange and correlation functionals and different basis sets all affect the predictions. For HNO calculations, among all 74 computational methods used in this work (see the Supporting Information for details), a new pure DFT method mPWVWN with a 6-311++G(2d,2p) basis was chosen on the basis of its best performance in predictions of experimental geometric parameters and vibrational frequencies<sup>80,81</sup> (vide infra). This mPWVWN method was then used in geometry optimizations and frequency calculations of all HNO, RNO, and NO heme model complexes investigated here (**2–7**, **13–16**), with the 6-311++G(2d,2p) basis for HNO and the first coordination shell atoms, while the rest of the atoms were treated with a 6-31G(d) basis for computational efficiency. This is designated as 6-311++G(2d,2p)|metal’s basis|6-31G(d) in this work. Among a number of all-electron and effective core potential basis sets examined here (see the Supporting Information for details), the use of the DGDZVP for Ru and Wachters’ for Fe was found to yield the best predictions of vibrational data. For calculations of the proton NMR chemical shifts,  $\delta_{\text{H}}$ , in the HNO moieties of the HNO metal complexes, we used the method that previously yielded excellent predictions of <sup>1</sup>H NMR shifts in various metal-containing systems,<sup>82</sup> that is, the B3LYP/6-311++G(2d,2p)|metal’s basis|6-31G(d) method. Ru and Fe were treated with the DGDZVP and LanL2DZ bases, respectively. In <sup>15</sup>N NMR property predictions, the OP86/6-311++G(2d,2p) method for the experimental reference system NH<sub>3</sub> and the OP86/6-311++G(2d,2p)|LanL2DZ|6-31G(d) method for iron porphyrin systems were chosen (see the Supporting Information for details). On the basis of these calculations for HNO and RNO heme model complexes as well as additional results in Supporting Information, we used the following methods for  $\nu_{\text{NO}}$ ,  $\delta_{\text{H}}$ , and  $\delta_{\text{N}}$  predictions in MbHNO models (**13–16**): mPWVWN/6-311++G(2d,2p)|Wachters|6-31G(d), B3LYP/6-311++G(2d,2p)|LanL2DZ|6-31G(d), and OP86/6-311++G(2d,2p)|LanL2DZ|6-31G(d), respectively.

## Results and Discussion

**Vibrational and Structural Properties in HNO and RNO Heme Model Complexes.** We first investigated HNO to see for this small molecule how well we can improve over the previous predictions of the geometric structures and vibrational frequencies,<sup>37</sup> which will build a basis for subsequent calculations for synthetic HNO metal complexes. Clearly, as seen from Tables 1 (selected results) and S1 (all results), the use of pure or hybrid DFT methods with different exchange and correlation functionals and different basis sets all affect the predictions. We first performed calculations with the widely used hybrid HF-DFT method B3LYP using a number of different basis sets (see Table S1), which resulted in large errors of 88–110 cm<sup>-1</sup> for  $\nu_{\text{NO}}$  predictions, as found in the previous report.<sup>37</sup> We then used

(57) Zhang, Y.; Sun, H. H.; Oldfield, E. *J. Am. Chem. Soc.* **2005**, *127*, 3652–3653.

(58) Reed, A. E.; Curtiss, L. A.; Weinhold, F. *Chem. Rev.* **1988**, *88*, 899–926.

(59) Becke, A. D. *J. Chem. Phys.* **1993**, *98*, 5648–5652.

(60) Adamo, C.; Barone, V. *J. Chem. Phys.* **1998**, *108*, 664–675.

(61) Becke, A. D. *Phys. Rev. A* **1988**, *38*, 3098–3100.

(62) Vosko, S. H.; Wilk, L.; Nusair, M. *Can. J. Phys.* **1980**, *58*, 1200–1211.

(63) Lee, C.; Yang, W.; Parr, R. G. *Phys. Rev. B* **1988**, *37*, 785–789.

(64) Perdew, J. P.; Zunger, A. *Phys. Rev. B* **1981**, *23*, 5048–5079.

(65) Perdew, J. P. *Phys. Rev. B* **1986**, *33*, 8822–8824.

(66) Becke, A. D. *J. Chem. Phys.* **1996**, *104*, 1040–1046.

(67) Perdew, J. P.; Burke, K.; Ernzerhof, M. *Phys. Rev. Lett.* **1996**, *77*, 3865–3868.

(68) Tao, J. M.; Perdew, J. P.; Staroverov, V. N.; Scuseria, G. E. *Phys. Rev. Lett.* **2003**, *91*, 4.

(69) Frisch, M. J.; et al. *Gaussian 03*, revision D.01; Gaussian, Inc.: Wallingford, CT, 2004.

(70) Gill, P. M. W. *Mol. Phys.* **1996**, *89*, 433–445.

(71) Perdew, J. P.; Burke, K.; Wang, Y. *Phys. Rev. B* **1996**, *54*, 16533–16539.

(72) Handy, N. C.; Cohen, A. J. *Mol. Phys.* **2001**, *99*, 403–412.

(73) Davidson, E. R. *Chem. Phys. Lett.* **1996**, *260*, 514–518.

(74) Wachters, A. J. *J. Chem. Phys.* **1970**, *52*, 1033–1036.

(75) <http://www.emsl.pnl.gov/forms/basisform.html>.

(76) Godbout, N.; Salahub, D. R.; Andzelm, J.; Wimmer, E. *Can. J. Chem.* **1992**, *70*, 560–571.

(77) Hay, P. J.; Wadt, W. R. *J. Chem. Phys.* **1985**, *82*, 270–283.

(78) Stevens, W. J.; Krauss, M.; Basch, H.; Jasien, P. G. *Can. J. Chem.* **1992**, *70*, 612–630.

(79) Leininger, T.; Nicklass, A.; Stoll, H.; Dolg, M.; Schwerdtfeger, P. *J. Chem. Phys.* **1996**, *105*, 1052–1059.

(80) Dalby, F. W. *Can. J. Phys.* **1958**, *36*, 1336–1371.

(81) Clough, P. N.; Thrush, B. A.; Ramsay, D. A.; Stamper, J. G. *Chem. Phys. Lett.* **1973**, *23*, 155–156.

(82) Zhang, Y.; Lewis, J. C.; Bergman, R. G.; Ellman, J. A.; Oldfield, E. *Organometallics* **2006**, *25*, 3515–3519.

**Table 1.** Errors in Selected Results of Geometry Optimizations and Frequency Calculations for HNO

entry <sup>a</sup>	DFT method	basis	$\Delta R_{\text{NO}}$ (Å)	$\Delta R_{\text{NH}}$ (Å)	$\Delta \nu_{\text{NO}}$ (cm <sup>-1</sup> )	$\Delta \nu_{\text{HNO}}$ (cm <sup>-1</sup> )
<i>b</i>	B3LYP	6-311G(2d,2p)	-0.010	0.000	90	73
<i>b</i>	BLYP	6-311G(2d,2p)	0.007	0.019	-6	-11
9	B3LYP	6-311++G(2d,2p)	-0.010	-0.003	88	65
18	mPW1PW91	6-311++G(2d,2p)	-0.018	-0.006	143	84
46	BVWN5	6-311G(2d,2p)	0.008	0.011	2	-6
56	mPWVWN5	6-311G(2d,2p)	0.007	0.011	3	-14
67	mPWVWN	6-311++G(2d,2p)	0.006	0.006	1	0

<sup>a</sup> The entry number corresponds to that in Table S1, which includes full results. <sup>b</sup> Reference 37.

**Table 2.** NMR, IR/Raman, Structural, and Charge Properties in Molecules 1–16

system		$R_{\text{NO}}$ (Å)	$R_{\text{NH}}$ (Å)	$R_{\text{MN}}$ (Å)	$\angle \text{H-N-O}$ (deg)	$\angle \text{M-N-O}$ (deg)	$\nu_{\text{NO}}$ (cm <sup>-1</sup> )	$\delta_{\text{H}}$ (ppm)	$\delta_{\text{N}}$ (ppm)	$Q_{\text{NO}}$ (e)	$Q_{\text{H}}$ (e)	ref
1 HNO	expt	1.211	1.063				1565					80, 81
	calc	1.217	1.069		108.6		1566	30.06	1237	-0.233	0.233	
2 Ru(TTP)(HNO)(1-MeIm)	expt						1380	13.64				33
	calc	1.248	1.039	1.940	112.0	132.1	1382	13.18		-0.383	0.284	
3 Ru(HNO)(‘py <sup>bu</sup> S <sub>4</sub> ’)	expt	1.242		1.875		130	1358	19.56				30
	calc	1.250	1.040	1.953	111.7	130.7	1370	19.98		-0.421	0.279	
4 Fe(TPP)(‘PrNO)(1-MeIm)	expt	1.24		1.81		122	1433					35
	calc	1.244		1.855		123.0	1428			-0.198		
5 Fe(OEP)(‘PrNO)(1-MeIm)	expt	1.26		1.80		123	1423					35
	calc	1.244		1.854		123.0	1429			-0.199		
6 Fe(TPP)(NO)(1-MeIm)	expt	1.182		1.750		138	1630					84, 85
	calc	1.189		1.747		140.6	1614			-0.057		
7 [Fe(OETPP)(NO)(1-MeIm)] <sup>+</sup>	expt	1.130		1.650		177.0	1871					86
	calc	1.151		1.653		179.9	1874			0.348		
8 NH <sub>3</sub>	expt		1.015						0.00			87
	calc		1.015						0.74			
9 Fe(TPP)(PhNO)(1-MeIm)	expt	1.254		1.800		124.8			605			34
	calc								616			
10 Fe(TPP)(PhNO)(py)	expt	1.249		1.819		123.9			607			34
	calc								632			
11 Fe(TPP)(NODMA)(py)	expt	1.252		1.859		119.8			607			34
	calc								590			
12 Fe(OEP)(PhNO)(1-MeIm)	expt	1.264		1.806		123.3			593			34
	calc								616			
MbHNO	expt	1.241		1.820		131.0	1385	14.80	661			22, 23
13 Fe(Por)(HNO)(5-MeIm)	calc	1.245	1.040	1.804	112.4	132.4	1400	15.42	607	-0.307	0.289	
14 Fe(Por)(HNO⋯H <sub>2</sub> O)(5-MeIm)	calc	1.252	1.038	1.795	111.5	133.8	1379	14.61	596	-0.304	0.303	
15 Fe(Por)(H <sub>2</sub> O⋯HNO)(5-MeIm)	calc	1.247	1.043	1.805	112.0	130.6	1400	15.54	643	-0.284	0.337	
16 Fe(Por)(H <sub>2</sub> O⋯HNO⋯H <sub>2</sub> O)(5-MeIm)	calc	1.253	1.042	1.800	111.2	131.6	1382	14.63	642	-0.323	0.340	

another hybrid method mPW1PW91, which contains more HF exchange component as compared to B3LYP to examine the effect of HF exchange on such kind of calculations. As shown in Table S1, results are even worse; for example, the errors in  $\nu_{\text{NO}}$  predictions are 143–170 cm<sup>-1</sup>. These results suggest that the methods with less or no HF exchange may perform better in the investigation of HNO vibrations, which was confirmed by additional pure DFT calculations (see Table S1). Among all 74 different methods examined here, a new pure DFT method mPWVWN with a 6-311++G(2d,2p) basis produces the best predictions with 1 and 0 cm<sup>-1</sup> errors for  $\nu_{\text{NO}}$  and  $\nu_{\text{HNO}}$ , and 0.006 Å deviations from experimental NO and NH bond lengths.<sup>80,81</sup> Interestingly, this method was also found to perform well in our recent investigation of other molecules.<sup>83</sup>

As shown in Table 2, for the only HNO heme model complex reported to date, Ru(TTP)(HNO)(1-MeIm) (**2**), an error of 2 cm<sup>-1</sup> was obtained for  $\nu_{\text{NO}}$ . We also investigated Ru(HNO)(‘py<sup>bu</sup>S<sub>4</sub>’) (**3**), which as compared to other known HNO metal complexes characterized by IR and NMR techniques<sup>24–29,31,32</sup> is closest to a heme model environment by having a relatively rigid ligand set in the equatorial plane and a nitrogen-coordinated ligand in the axial

position. An error of 12 cm<sup>-1</sup> is much improved over the 155 cm<sup>-1</sup> error in the previous work.<sup>30</sup> In addition, we performed the first computational vibrational analysis of RNO heme model systems: Fe(TPP)(‘PrNO)(1-MeIm) (**4**) and Fe(OEP)(‘PrNO)(1-MeIm) (**5**), for which the predicted  $\nu_{\text{NO}}$  values deviate from experiment by -5 and 6 cm<sup>-1</sup>, respectively. For comparison, we also investigated the ferrous and ferric NO heme models: Fe(TPP)(NO)(1-MeIm) (**6**) and [Fe(OETPP)(NO)(1-MeIm)]<sup>+</sup> (**7**), for which the predicted geometric parameters and NO vibrations are again in good accord with experiment,<sup>84–86</sup> Table 2. Now, for all HNO, RNO, and NO systems (**1–7**) investigated here, as shown in Figure 2A–C, there are good agreements between theory and experiment:  $R^2 = 0.968$  and SD = 0.008 Å for  $R_{\text{NO}}$ ,  $R^2 = 0.978$  and SD = 0.020 Å for  $R_{\text{MN}}$ , and  $R^2 = 0.999$  and SD = 0.9° for  $\angle \text{M-N-O}$ . In addition, as demonstrated in Figure 3A, an excellent agreement between computational and experimental  $\nu_{\text{NO}}$  data can be found with  $R^2 = 0.998$

(84) Wyllie, G. R. A.; Schulz, C. E.; Scheidt, W. R. *Inorg. Chem.* **2003**, *42*, 5722–5734.

(85) Praneeth, V. K. K.; Nather, C.; Peters, G.; Lehnert, N. *Inorg. Chem.* **2006**, *45*, 2795–2811.

(86) Ellison, M. K.; Schulz, C. E.; Scheidt, W. R. *J. Am. Chem. Soc.* **2002**, *124*, 13833–13841.

(83) Ling, Y.; Zhang, Y. *J. Phys. Chem. A* **2009**, *113*, 5993–5997.

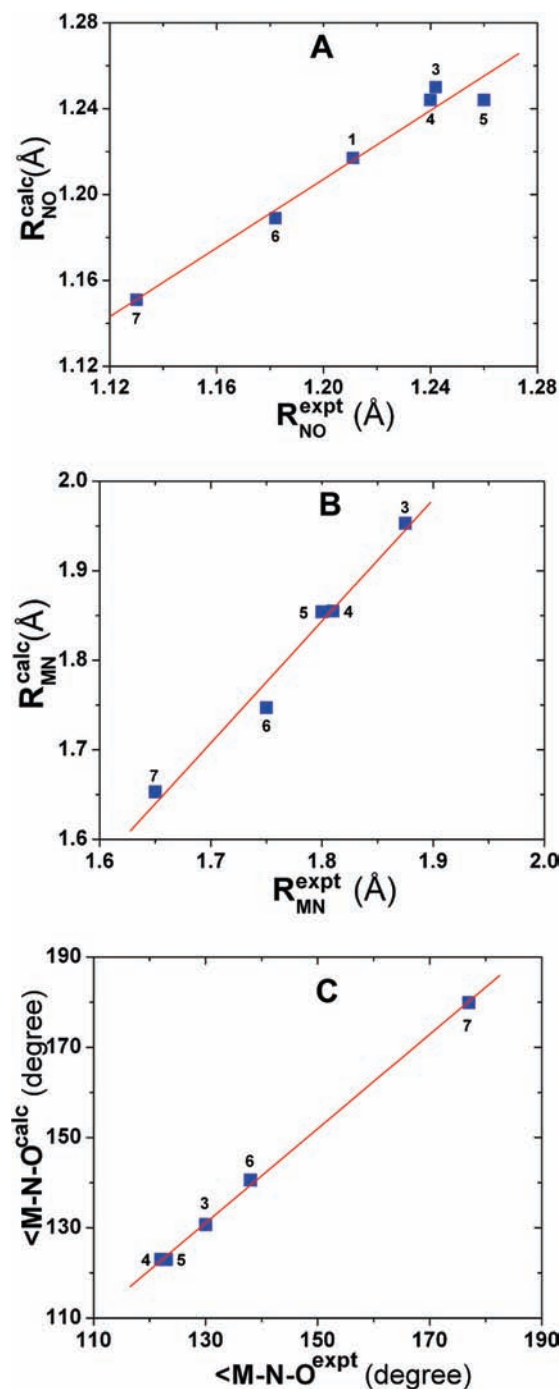


**Figure 2.** Computed versus experimental geometric parameters: (A) NO bond lengths; (B) MN bond lengths; and (C)  $\angle$ M–N–O bond angles.

and a SD = 9 cm<sup>-1</sup>, or 1.8% of the whole 513 cm<sup>-1</sup> range seen experimentally. These results indicate that the new pure DFT method mPWVWN is able to yield accurate geometries and NO vibrations in a number of HNO, RNO, and NO metalloporphyrins.

To further compare with the performance of this new mPWVWN method, additional calculations of the HNO, RNO, and NO heme models (2–4, 6, 7) using the next two favorable methods BVWN5/6-311G(2d,2p) and mPWVWN5/6-311G(2d,2p) were also carried out. These two methods result in errors of 2

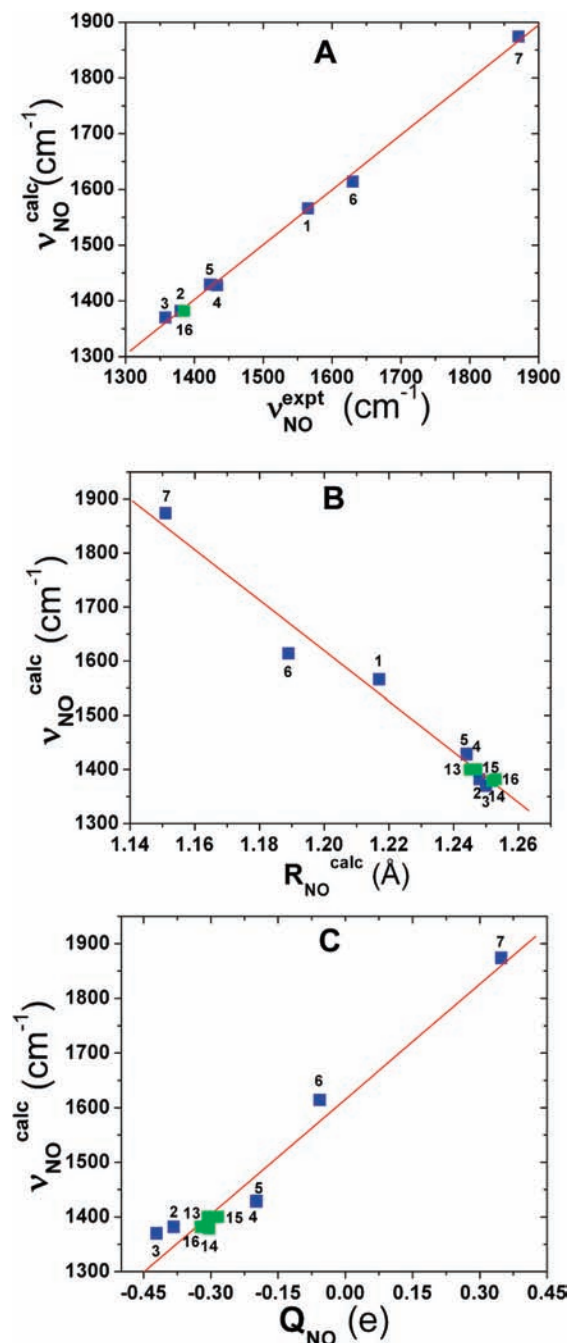


**Figure 3.** (A) Computed versus experimental NO vibrational frequencies in 1–7 and MbHNO model 16. (B) Calculated NO vibrational frequencies versus NO bond lengths in 1–7 and 13–16. (C) Calculated NO vibrational frequencies versus NPA charges of NO in metal complexes 2–7 and 13–16. Green data points are for MbHNO models.

and 3 cm<sup>-1</sup> for  $\nu_{\text{NO}}$  predictions of HNO, respectively, as compared to the 1 cm<sup>-1</sup> error from using the mPWVWN/6-311++G(2d,2p) method; see Table 1. As shown in Table S3, their mean absolute errors of  $\nu_{\text{NO}}$  predictions for the metal complexes are 12.8 cm<sup>-1</sup>, which is ca. 70% larger than that from using the mPWVWN method described above for the same set of metal complexes, 7.6 cm<sup>-1</sup>. These results further support the use of the new pure DFT method mPWVWN in investigating HNO, RNO, and NO heme systems.

As shown in Table 2, both experimental and computational results show that the NO vibrations in these three types of NO-containing heme complexes follow a general trend of NO >

(87) Jameson, C. J.; Jameson, A. K.; Oppunggu, D.; Willie, S.; Burrell, P. M.; Mason, J. *J. Chem. Phys.* **1981**, *74*, 81–88.

RNO > HNO complexes. Interestingly, the computational results offer a couple of insights into the origin of this trend. As demonstrated in Figure 3B, there is an excellent linear QSOR between  $\nu_{\text{NO}}$  and  $R_{\text{NO}}$  with  $R^2 = 0.977$  in all of these NO-containing molecules with a trend of  $\text{NO} < \text{RNO} < \text{HNO}$  complexes for NO bond lengths, which supports the opposite trend seen for NO vibrational frequencies. This also indicates that NO vibrations are mainly local effects of the NO bonds and the NO bond lengths may be deduced directly from using the NO vibrational frequencies in all of these NO-containing systems, including some MbHNO models (vide infra). In addition, an excellent relationship between NO vibrational frequencies and NPA charges of the NO groups in all of the metal complexes ( $Q_{\text{NO}}$ ) with  $R^2 = 0.953$  was found, as shown in Figure 3C. This shows that there is a common bonding behavior in the NO moieties in all of these different NO-containing systems: with more electrons populated in the antibonding  $\pi_{\text{NO}}^*$  orbital, the NO bonds become weakened, resulting in longer NO bond lengths and smaller NO vibrational frequencies. HNO and RNO have an extra electron as compared to NO, which results in weaker NO bonds and consequently smaller NO vibrational frequencies seen in HNO and RNO heme model complexes as compared to NO heme systems. The negative charges of HNO moieties in the HNO heme model complexes (see Table 2) indicate that HNO acts as a  $\pi$  acid, receiving back-donation from the metal center, which is the same as in other nonheme type HNO metal complexes.<sup>27</sup> For the isoelectronic HNO and RNO species, the observed smaller NO vibrational frequencies in HNO metal complexes as compared to RNO complexes suggest that HNO is a stronger  $\pi$  acid than RNO, in agreement with the calculated charges of NO groups in these systems.

#### NMR Properties in HNO and RNO Heme Model Complexes.

As shown in Table 2, for the two synthetic HNO complexes **2** and **3**, the errors in proton NMR shift predictions are 0.46 and 0.42 ppm, respectively. These results indicate that in these first reports of the  $^1\text{H}$  NMR shift predictions for HNO metal complexes, the errors are similar to those seen with other metal complexes using basically the same method.<sup>82</sup> Indeed, as demonstrated in Figure 4A, there is an excellent agreement between experiment and calculation for all of these systems with  $R^2 = 0.990$  and  $\text{SD} = 0.52$  ppm, or 2.6% of the whole 19.89 ppm range seen experimentally. This suggests that the method used here works well for a number of different metal complexes.

We then moved to the predictions of  $^{15}\text{N}$  NMR chemical shifts in RNO heme model complexes.<sup>34</sup> For the experimental reference system  $\text{NH}_3$  (**8**), the predicted shift by using the OP86/6-311++G(2d,2p) method has an error of 0.74 ppm as compared to the experimental result.<sup>87</sup> For the RNO heme model complex **9**, an error of 11 ppm was obtained, Table 2, which is much improved over the previously reported error of 23 ppm.<sup>34</sup> This kind of computational error is close to that seen in solution  $^{15}\text{N}$  NMR experiments for investigating protein systems due to a number of experimental effects.<sup>88</sup> An overall comparison with the experimental  $^{15}\text{N}$  NMR shifts for **8–12** shows  $R^2 = 0.996$  and  $\text{SD}$  of 19 ppm or 3.1% of the studied experimental range. In addition, the predicted  $^{15}\text{N}$  NMR chemical shift tensor elements (see the Supporting Information for details) are also in excellent agreement with experimental data, with  $R^2 = 0.991$  and 3.5% error over the entire experimental range of 1281 ppm. These results are demonstrated in Figure 4B.

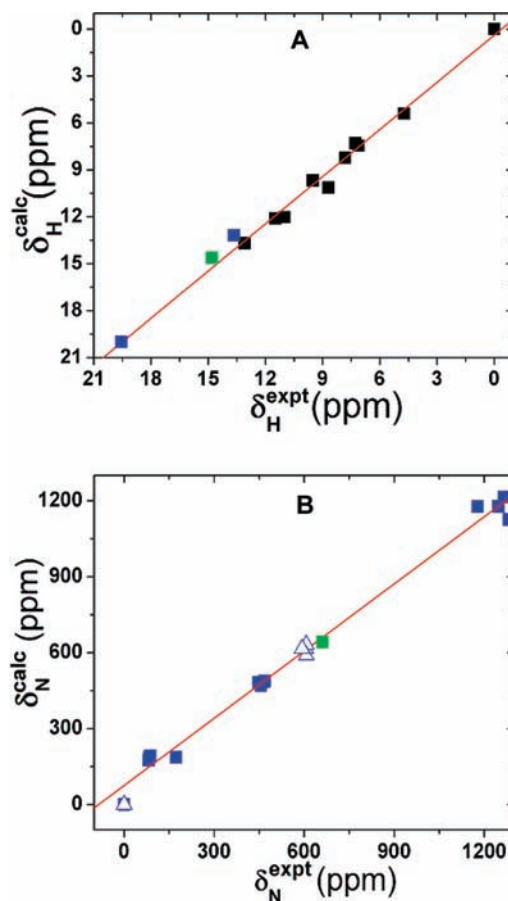


**Figure 4.** (A) Computed versus experimental  $^1\text{H}$  NMR chemical shifts. Blue, black, and green data points are for synthetic HNO metal complexes, other metal complexes, and ligands from ref 82 and MbHNO model **16**. (B) Computed versus experimental  $^{15}\text{N}$  NMR chemical shift tensor results. The triangle data points are the corresponding isotropic values, and the green data point is for MbHNO model **16**.

As compared to the predicted  $^1\text{H}$  NMR shift of 30.06 ppm and  $^{15}\text{N}$  NMR shift of 1237 ppm in free HNO, both the proton and the nitrogen NMR shifts in HNO metal complexes are much upfield, suggesting a strong effect from metal coordination. As shown in Table 2, large electron densities in the HNO moiety ( $Q_{\text{NO}} + Q_{\text{H}}$ ) in HNO metal complexes were found in comparison to that in free HNO, which result in larger NMR chemical shieldings and consequently the smaller NMR chemical shifts seen experimentally in HNO metal systems. The extra electron densities gained through the metal coordination in these HNO metal complexes reflect the  $\pi$ -acidity nature of HNO in these complexes. The strong  $\pi$ -acid effect of HNO seen from these NMR results is also consistent with the above results and discussion on NO vibrations in HNO metal complexes.

**MbHNO Model Calculations.** To obtain a preliminary understanding of the structural effects, especially the previously unexplored hydrogen-bond effect in MbHNO on the three spectroscopic “fingerprints”,  $\nu_{\text{NO}}$ ,  $\delta_{\text{H}}$ , and  $\delta_{\text{N}}$ , we carried out a series of calculations on the following models:  $\text{Fe}(\text{Por})(\text{HNO})-(5\text{-MeIm})$  (**13**),  $\text{Fe}(\text{Por})(\text{HNO}\cdots\text{H}_2\text{O})(5\text{-MeIm})$  (**14**),  $\text{Fe}(\text{Por})(\text{H}_2\text{O}\cdots\text{HNO})(5\text{-MeIm})$  (**15**), and  $\text{Fe}(\text{Por})(\text{H}_2\text{O}\cdots\text{HNO}\cdots\text{H}_2\text{O})(5\text{-MeIm})$  (**16**). As shown in Figure 1, in these models, the HNO adopts a perpendicular conformation with respect to the axial His ligand (modeled as 5-MeIm here), since this was found in a previous experimental work<sup>21</sup> and there is no significant difference between the perpendicular and parallel conformations

(88) Mason, J.; Larkworthy, L. F.; Moore, E. A. *Chem. Rev.* **2002**, *102*, 913–934.

in both geometries and predicted spectroscopic properties.<sup>37</sup> As the HNO molecule has both terminal hydrogen and oxygen atoms available to form hydrogen bonds, models **14**, **15**, and **16** were used to investigate the effects of HNO act as a hydrogen-bond acceptor, hydrogen-bond donor, and both. Here, the water molecule is used as a hydrogen-bond probe because of its simplicity, capability of acting as both hydrogen-bond donor and acceptor, and viability in the protein systems.

As shown in Table 2, for the hydrogen-bond free model **13**, although the  $\nu_{\text{NO}}$  calculation error has been greatly reduced in comparison to an early work,<sup>37</sup> the overall errors in these three spectroscopic properties are large enough to preclude this model for MbHNO. Interestingly, when HNO acts as a hydrogen-bond acceptor (**14**), both  $\nu_{\text{NO}}$  and  $\delta_{\text{H}}$  predictions of 1379  $\text{cm}^{-1}$  and 14.61 ppm become close to the experimental data of 1385  $\text{cm}^{-1}$  and 14.80 ppm.<sup>22,23</sup> However, the  $^{15}\text{N}$  NMR shift prediction error is enlarged, indicating that, although this model corrects some problems, it still misses one or more essential structural feature(s) in MbHNO. In the case of HNO acting as a hydrogen-bond donor (**15**), an exactly opposite phenomenon was observed; see Table 2. The calculated  $^{15}\text{N}$  NMR chemical shift was improved by 36 ppm, yet there is no improvement or even a little deterioration for  $\nu_{\text{NO}}$  and  $\delta_{\text{H}}$  predictions. These results suggest that in MbHNO, these two hydrogen-bonding structural effects may be applicable at the same time. Indeed, as shown for the dual hydrogen-bond model (**16**) in Table 2, all of these three characteristic spectroscopic property predictions were improved simultaneously. This can also be seen from Figures 3 and 4 for  $\nu_{\text{NO}}$ ,  $\delta_{\text{H}}$ , and  $\delta_{\text{N}}$  plots, where the predicted values of the dual hydrogen-bond model (**16**) fit well with results of related HNO/RNO systems. This suggests that the HNO moiety in MbHNO may be involved in two hydrogen bonds as found in the HNO dimer<sup>89</sup> and synthetic HNO metal complex.<sup>30</sup> In MbHNO, the distal His residue and a possible water molecule in the active site can form the two hydrogen bonds with HNO. Because the experimental NMR studies indicate that a wide range of active site residues may be involved in the interactions with HNO,<sup>21</sup> an extensive examination of these effects in MbHNO toward an accurate picture of the HNO interactions in a heme protein environment is under investigation in our group.

The capability of forming dual hydrogen bonds for HNO may provide a basis for the unusual stability of MbHNO observed experimentally.<sup>11</sup> As shown in Figure 5, the HOMOs and LUMOs are essentially the same for all MbHNO models studied here (**13**–**16**), with a  $\sigma_{\text{NH}}$  orbital acting as the hydrogen-bond donor and a  $\pi_{\text{NO}}^*$  orbital acting as the hydrogen-bond acceptor. The hydrogen-bond distances of  $\text{O}_{\text{water}} \cdots \text{H}_{\text{HNO}}$  are 2.028 Å in **15** and 2.012 Å in **16**, and the distances of  $\text{O}_{\text{HNO}} \cdots \text{H}_{\text{water}}$  are 2.072 Å in **14** and 2.070 Å in **16**. Clearly, the hydrogen-bond distances in the dual hydrogen-bond model **16** are shortened in comparison to those in the single hydrogen-bond models **14** and **15**. This suggests that the hydrogen bonds are not simply added together in **16**, but have a synergetic, strengthening effect, consistent with the additional stabilization energies of 8–9 kcal/mol in **16** than in **14** and **15**. This kind of dual hydrogen-bonding capability of HNO is unique and has not been seen in heme protein complexes with other small molecules such as  $\text{O}_2$ , which

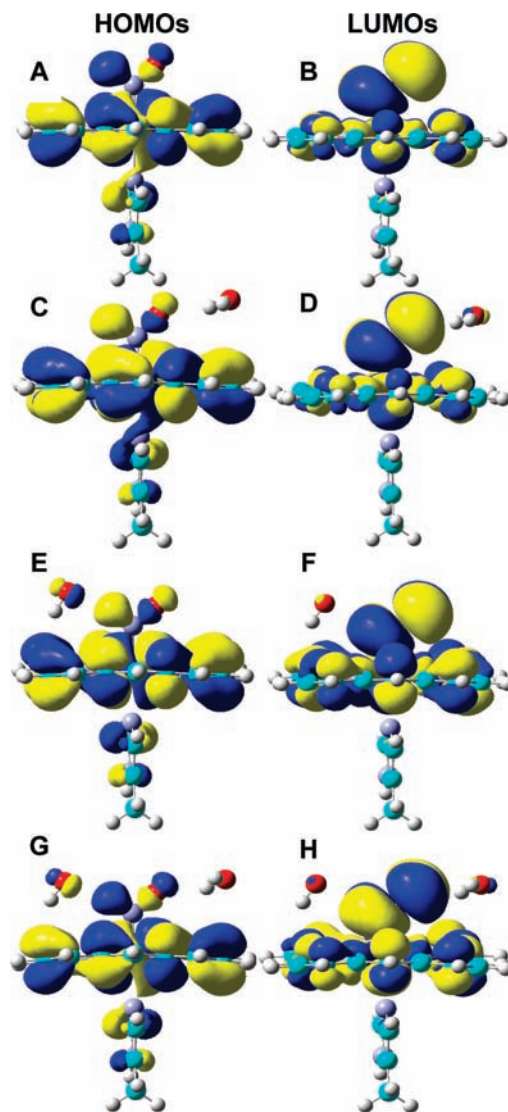


**Figure 5.** Isosurface representations of HOMOs and LUMOs for **13** (A,B), **14** (C,D), **15** (E,F), and **16** (G,H), respectively, with contour values =  $\pm 0.01$  au.

may be responsible for the stronger binding affinity of Mb for HNO than the native substrate dioxygen.<sup>11</sup>

## Conclusion

The results we have described above are of interest for a number of reasons. First, on the basis of a comprehensive methodological investigation, a new pure DFT method mP-WVWN was found to yield excellent predictions of key geometric parameters around the NO groups ( $R_{\text{NO}}$ ,  $R_{\text{MN}}$ ,  $\angle\text{M-N-O}$ ) in the HNO, RNO, and NO heme model complexes with  $R^2 = 0.968$ – $0.999$ . Second, for the three characteristic spectroscopic properties  $^1\text{H}$  and  $^{15}\text{N}$  NMR chemical shifts and NO vibrational frequencies in synthetic HNO and RNO heme complexes, excellent correlations with experimental results were found with  $R^2 = 0.990$ – $0.998$ . Third, an excellent linear QSOR was found between  $\nu_{\text{NO}}$  and  $R_{\text{NO}}$  with  $R^2 = 0.977$  in all of the HNO, RNO, and NO heme model complexes investigated here, which may help deduce the NO bond lengths from experimental NO vibrational data.  $\nu_{\text{NO}}$  data have a general trend of  $\text{NO} > \text{RNO} > \text{HNO}$  complexes, resulting from the opposite trend of the electron populations in the antibonding NO orbitals.

(89) Liu, Y.; Liu, W. Q.; Li, H. Y.; Liu, J. G.; Yang, Y. *J. Phys. Chem. A* **2006**, *110*, 11760–11764.



Investigations of the NMR and IR/Raman spectroscopic data in HNO metal complexes show that HNO is a strong  $\pi$ -acid. Fourth, we performed the first quantum chemical investigation of the hydrogen-bond effect on HNO in MbHNO models. On the basis of comparisons with experimental  $^1\text{H}$  and  $^{15}\text{N}$  NMR results and NO vibrational frequency in MbHNO, a dual hydrogen-bond mode for HNO was proposed. The enhanced stability from this dual hydrogen bonding may account for the unusual stability of MbHNO observed experimentally. Taken together, these results are of broad general interest because they represent the first accurate quantum chemical investigations of some characteristic NMR and IR/Raman spectroscopic results in HNO and RNO heme complexes, which should facilitate spectroscopic characterizations and structural investigations of HNO and RNO heme proteins and models.

**Acknowledgment.** This work was supported by the NIH grant GM-085774 and NSF EPSCoR grant OIA-0556308. We are also grateful to the Mississippi Center of Supercomputing Research and USM Vislab for generous use of their computing facilities. We thank Patrick J. Farmer for providing the correct experimental  $^{15}\text{N}$  NMR chemical shift reference information for MbHNO. We also thank Weston T. Borden, Eric Oldfield, and reviewers for helpful comments.

**Supporting Information Available:** Full citation of ref 69 and additional computational details and results (Tables S1–S18). This material is available free of charge via the Internet at <http://pubs.acs.org>.

JA907342S